Potential mechanisms underlying podophyllotoxin-induced cardiotoxicity in male rats: toxicological evidence chain (TEC) concept

Kaiyue Ma[1†], Lu Sun[2†], Chunxue Jia[1], Hongqian Kui[1], Jiaqi Xie[1], Shidan Zang[1], Shixin Huang[3], Jinfeng Que[1], Chuanxin Liu[4]* and Jianmei Huang[1]*

[1]School of Chinese Materia Medica, Beijing University of Chinese Medicine, Beijing, China, [2]College of Chinese Materia Medica and Food Engineering, Shanxi University of Chinese Medicine, Jinzhong, China, [3]Eye Hospital China Academy of Chinese Medical Sciences, Beijing, China, [4]Luoyang Key Laboratory of Clinical Multiomics and Translational Medicine, Henan Key Laboratory of Rare Diseases, Endocrinology and Metabolism Center, The First Affiliated Hospital, and College of Clinical Medicine of Henan University of Science and Technology, Luoyang, China

Introduction: Podophyllotoxin (PPT) is a high-content and high-activity compound extracted from the traditional Chinese medicinal plant *Dysosma versipellis* (*DV*) which exhibits various biological activities. However, its severe toxicity limits its use. In clinical settings, patients with *DV* poisoning often experience adverse reactions when taking large doses in a short period. The heart is an important toxic target organ, so it is necessary to conduct 24-h acute cardiac toxicity studies on PPT to understand its underlying toxicity mechanism.

Methods: Based on the concept of the toxicological evidence chain (TEC), we utilized targeted metabolomic and transcriptomic analyses to reveal the mechanism of the acute cardiotoxicity of PPT. The manifestation of toxicity in Sprague-Dawley rats, including changes in weight and behavior, served as Injury Phenotype Evidence (IPE). To determine Adverse Outcomes Evidence (AOE), the hearts of the rats were evaluated through histopathological examination and by measuring myocardial enzyme and cardiac injury markers levels. Additionally, transcriptome analysis, metabolome analysis, myocardial enzymes, and cardiac injury markers were integrated to obtain Toxic Event Evidence (TEE) using correlation analysis.

Results: The experiment showed significant epistaxis, hypokinesia, and hunched posture in PPT group rats within 24 h after exposure to 120 mg/kg PPT. It is found that PPT induced cardiac injury in rats within 24 h, as evidenced by increased serum myocardial enzyme levels, elevated concentrations of cardiac injury biomarkers, and altered cardiac cell morphology, all indicating some degree of cardiac toxicity. Transcriptome analysis revealed that primary altered metabolic pathway was arachidonic acid metabolism after PPT exposure. Cyp2e1, Aldob were positively correlated with differential metabolites, while DHA showed positive correlation with differential genes Fmo2 and Timd2, as well as with heart injury markers BNP and Mb.

Conclusion: This study comprehensively evaluated cardiac toxicity of PPT and initially revealed the mechanism of PPT-induced acute cardiotoxicity, which involved oxidative stress, apoptosis, inflammatory response, and energy metabolism disorder.

1 Introduction

Podophyllotoxin (PPT) is a high-content and high-activity compound extracted from a plant in traditional Chinese medicine (TCM), *Dysosma versipellis* (*DV*). Its content in the *DV* raw drug can reach up to 9%. PPT exhibits various biological activities, such as anti-tumor, antiviral, and anti-inflammatory effects. In particular, its anti-tumor activity is evidenced by the inhibition of the proliferation of non-small-cell lung cancer, human oral squamous cell carcinoma, and other cancer cells (Pathak et al., 2022; Tan et al., 2018; Zhao et al., 2021). However, the toxicity and serious gastrointestinal adverse reactions of PPT, as well as the lack of specific drugs after poisoning, limit its clinical application (Kong et al., 2023). The toxicity caused by *DV* involves multiple organs, with the heart as an important target. Thus, PPT may cause damage to the heart, but this has not been confirmed, and the related toxicity mechanisms are not yet clear. Therefore, there is a need for a systematic and comprehensive analysis to explore the cardiotoxicity and mechanism of PPT action to facilitate its treatment utility.

The toxicological evidence chain (TEC) framework was first proposed and applied to research potential toxic material bases and mechanisms of compounds and natural drugs in 2019 by our research group (Liu et al., 2020). The current TEC framework comprises four core contents. Injury phenotype evidence (IPE) involves examining the overall animal level behavioral status after administering TCM in model animals and qualitatively and quantitatively characterizing the toxic behavior and toxic manifestations of animals. Harmful ingredients evidence (HIE) examines the drug-derived component or substance basis related to toxic outcomes. Toxic events evidence (TEE) involves obtaining endogenous differences in key targets, metabolic small molecules, and signal transduction in the process of toxicity. Adverse outcomes evidence (AOE) involves investigating the substantial detriment to target organs (Kong et al., 2022; Duan et al., 2024). This study was based on the TEC method, where we constructed a TEC framework for PPT and demonstrated the dynamic relationship between damage events and toxicity effects. The combined application of high-throughput omics technology provides guidance for comprehensive and multi-angle toxicity assessment. Transcriptomics uses high-throughput sequencing technology to compare normal and exposed individuals, identify different messenger ribonucleic acids related to toxicity, and discover potential genomic biomarkers of PPT cardiotoxicity. Targeted metabolomics uses highly sensitive detection methods to quantitatively analyze specific endogenous small-molecule compounds and to screen potential biomarkers related to cardiotoxicity.

In this study, we first determined the changes in epimorphology, serum biochemical indicators, cardiac injury markers, and cardiac tissue morphology in Sprague–Dawley (SD) male rats exposed to PPT. Subsequently, transcriptome characteristics and arachidonic acid-targeted metabolomic profiles were revealed, utilizing heart transcriptomics and targeted metabolomics approaches. Finally, transcriptome analysis, metabolome analysis, myocardial enzymes, and cardiac injury markers were integrated to explore the cardiotoxic mechanism of PPT.

2 Materials and methods

2.1 Reagents and materials

PPT (≥ 98%, 518-28-5) was purchased from Shanghai YUANYE Biotechnology Co., Ltd. In animal experiments, pentobarbital (Pentobarbital Sodium, P3761, Sigma, United States) was used to induce anesthesia, and sodium chloride (AR, S24119, Shanghai YUANYE Biotechnology Co., Ltd.) and 4% paraformaldehyde (R20486, 500 mL, Shanghai YUANYE Biotechnology Co., Ltd.) were used to wash and fix the hearts of the rats. ELISA kits for rat myoglobin (MYO/MB), rat brain natriuretic peptide/brain natriuretic peptide (BNP), rat cardiac troponin I (cTnI), and rat N-terminal pro-brain natriuretic peptide (NT-proBNP) were purchased from Jiangsu Meimian Industrial Co. Ltd. (batch numbers 2023082415R, 2023082467, 2023082450R, and 2023082429R, respectively). The mobile phases were acetonitrile (LC-MS, 192552, Thermo Fisher, United States), formic acid (LC-MS, 225583, Thermo Fisher, United States), methanol (LC-MS, 190379, Thermo Fisher, United States), and ultra-pure water from the Milli-Q Integral water purification system (Millipore, United States).

2.2 Toxicological research on cardiotoxicity induced by PPT (IPE and AOE)

2.2.1 Animal handling

Forty specific-pathogen-free (SPF) male SD rats weighing 230 ± 10 g and aged 7–8 weeks were purchased from Beijing Vital River Laboratory Animal Technology Co., Ltd., license number SCXK (Beijing-2021-0006), and raised in the Animal Laboratory of Liangxiang Campus, Beijing University of Chinese Medicine. The rats were fed under controlled environmental conditions with a 12-h day–night cycle, an ambient temperature of 23°C ± 2°C, and an ambient humidity of 35% ± 5%, with adaptive feeding for 3 days. Rats were randomly divided into two groups: blank control group (CON) and podophyllotoxin-treated group (PPT). The dosage of each group is

TABLE 1 Administration scheme of cardiotoxicity induced by PPT in rats.

Group	Number	Drug	Dose	Administration method	Exposure period (d)
CON	20	Ultra-pure water	1 mL/d	i.g., Single-dose administration	1
PPT	20	PPT solution	120 mg/kg		1

shown in Table 1. After administration, pentobarbital sodium was injected to anesthetize the rats, and their hearts were removed. Animal experiment protocols were approved by the Animal Ethics Committee of Beijing University of Chinese Medicine (BUCM-2023042701-2049). All experimental procedures were conducted following the Chinese national legislation and local guidelines.

2.2.2 Drug preparation

Drug solutions with a concentration of 100 mg/mL were prepared and diluted to the dose required for administration. In brief, we accurately weighed the appropriate amount of PPT, dissolved it in ultra-pure water as required, stored it in a refrigerator at 4 °C, and thawed it at room temperature before use. The solution for the blank control group was ultra-pure water. To ensure uniformity of gavage, we administered PPT to rats one by one and vortexed the PPT solution for 30 s to 1 min each time to ensure a uniform suspension.

2.2.3 Acute cardiac injury phenotype induced by PPT

After the CON and PPT groups were administered the drugs/blank, the rats' general behavior, appearance changes, general morphological changes, and deaths were observed, including changes in eye color, paws, and hair, bleeding, and the occurrence of diarrhea (Supplementary Table S1). Body weight changes were recorded every hour 0–4 h after administration, every 2 h 5–12 h after administration, and every 12 h 13–24 h after administration (GB/T 21757-2008, 2008). After administering the corresponding medication by gavage to the corresponding group of rats for 24 h, blood was drawn from the abdominal aorta. After blood collection, physiological saline was perfused from the liver at 0 °C without touching the heart until the lungs turned white. The rat heart was immediately collected and weighed to calculate its organ indexes.

2.2.4 Detection of myocardial enzyme and cardiac injury markers

The whole blood (8–10 mL) in a general vacuum tube was centrifuged once at 3,500 rpm, 4 °C for 15 min. The supernatant was stored in a refrigerator at −80 °C until myocardial enzymes biochemical parameters related to cardiac function were detected, including aspartate aminotransferase (AST), creatine kinase (CK), creatine kinase-MB isoenzyme (CK-MB), lactate dehydrogenase (LDH), and α-hydroxybutyrate dehydrogenase (α-HBD), as well as cardiac injury markers including brain natriuretic peptide/brain natriuretic peptide (BNP), cardiac troponin I (cTnI), myoglobin (MYO/MB), and N-terminal pro-brain natriuretic peptide (NT-proBNP). Mb, cTnI, BNP, and NT pro-BNP in blood were quantified by the ELISA kit following the manufacturer's instructions, and the optical density of each sample was measured at 450 nm. Finally, the levels of BNP, NT-pro BNP, Mb, and cTnI were quantified by the standard curve and expressed in ng/L.

2.2.5 Examination of pathological changes

In a 0 °C environment, the heart tissue was divided into three equal parts after clipping off the excess arterial and venous blood vessels. The apex of the heart, which is the lowest part, contains only the left ventricle. The middle part includes the left ventricle, right ventricle, and interventricular septum. The uppermost part comprises the left atrium, right atrium, and interatrial septum. The apex of the hearts of each group of rats was immersed in 4% paraformaldehyde for subsequent pathological evaluation. The remaining two parts were quickly stored at −80 °C. The middle part of the heart was used for transcriptome and arachidonic acid-targeted metabolomic studies. The apex of the hearts of each group of rats was stained with hematoxylin–eosin (H&E) to obtain sections for pathological assessment. Morphological and pathological observation and analysis were performed under a microscope to judge the structural effects of PPT on the heart tissue.

2.3 Transcriptome analysis for PPT-induced cardiotoxicity

2.3.1 RNA extraction, library construction, and sequencing

Heart tissue cells from eight rats each in the CON and PPT groups were selected for transcriptomic analysis. Total RNA was isolated from myocardial cells using the TRNzol Universal RNA Sample Preparation Kit (Invitrogen, United States) following the manufacturer's instructions. Nanodrop 2000 (NanoDrop, Wilmington, DE, United States) was used to detect the concentration and purity of the extracted RNA. RNA integrity was detected by agarose gel electrophoresis, and the RIN value was determined on an Agilent 2100 system (Agilent Technologies, CA, United States). The total amount of RNA required was ≥1 μg for a single database establishment. Sequencing libraries were constructed using Illumina Truseq™ RNA library Prep kit (Illumina, Nebraska, United States) following the manufacturer's protocol.

2.3.2 Data processing and enrichment analysis

Differential expression analysis was conducted using DESeq2 software (1.20.0). Significant differentially expressed genes (DEGs) between groups were determined using the following criteria: $p \leq 0.05$ and $|\log_2 \text{Fold Change}| \geq 1$. Functional enrichment analysis, including Gene Ontology (GO) and Kyoto Encyclopedia of Genes and Genomes (KEGG), were performed to identify significant GO terms and enriched metabolic pathways related to the DEGs ($p \leq 0.05$) compared with the whole-transcriptomic background. GO functional enrichment and KEGG pathway analysis were conducted using the clusterProfiler package (3.4.4).

2.4 Arachidonic acid metabolism-based targeted metabolomics study on cardiotoxicity induced by PPT

2.4.1 Sample pretreatment

Heart samples from rats in the CON ($n = 8$) and PPT ($n = 8$) groups were randomly selected and thawed at 4 °C before metabolomic analysis. Each tissue sample (50 mg) was mixed with a ten-fold amount of the BHT protein precipitant and 10 μL of the internal standard at a concentration of 1 μg/mL, mixed for 20 s, and centrifuged at 4 °C and 14000 rcf for 10 min for protein precipitation. Next, the supernatant (400 μL) was purified using an Oasis HLB 96-well plate. The eluent was dried under nitrogen gas and subjected to UPLC-Q-TOF/HRMS analysis for metabolomics evaluation. An equal amount (10 μL) from each sample was mixed with the QC sample to monitor the repeatability and stability of the instrument.

2.4.2 UPLC-QTRAP-MS analysis

Chromatographic separation was achieved using an Agilent 1290 Infinity LC system (Agilent, United States) with a Waters ACQUITY UPLC BEH C18 (1.7 μm, 2.1 × 50 mm) chromatographic column at a maintained temperature of 35 °C. The tissue sample injection volume was set to 2 μL, and the temperature of the autosampler was fixed at 4 °C. The gradient mobile phase was a mixture of 0.1% formic acid in water (phase A) and 0.1% formic acid in acetonitrile (phase B), which was pumped at a flow rate of 0.4 mL/min. The optimal elution procedure of phase B was set as follows: 0–1 min, 30%; 1–9 min, 30%–90%; 9–11 min, 90%; 11–11.1 min, 90%–20%; 11.1–14 min, 20%. Mass spectrometry data detection and acquisition was performed on the QTRAP mass spectrometry (5500 QTRAP, SCIEX, United States, ESI) instrument in the MRM mode. The ion pair information of all 15 arachidonic acid metabolites is shown in Supplementary Table S2. Mass spectra were obtained in the negative ion mode. Mass spectrometry parameters were set as follows: source temperature, 500°C; Ion Source Gas1 (Gas1), 50; Ion Source Gas2 (Gas2), 50; Curtain gas (CUR), 30; Ion Spray Voltage Floating (ISVF), −4500 V.

2.4.3 Methodological study

Ion flow chromatography (XIC) is used to extract a standard sample of metabolites to determine whether each can be quantitatively analyzed by mass spectrometry. Six QC samples were injected continuously for analysis, and RSD values of peak area and retention time were calculated to assess the stability and repeatability of the experiment. The linear range of 15 metabolites was determined by a linear test.

2.4.4 Data processing

The chromatographic peak area and retention time were determined using Multiquant 3.0.2 software (SCIEX, United States). Metabolite identification and absolute quantification were performed using the standard substance of the 15 arachidonic acid metabolites to correct retention time. Differential metabolites with fold change >1.5 or <0.67 with $p < 0.05$ were selected as candidates. R (version 4.0.3) and R packages were used for all multivariate data analyses and modeling. Data were mean-centered using Pareto scaling. Models were built on orthogonal partial least-squares discriminant analysis (OPLS-DA) and partial least-squares discriminant analysis (PLS-DA). All the models evaluated were tested for overfitting using permutation test methods.

2.5 Statistical analysis

Descriptive statistics were used to characterize the groups studied. The mean and standard deviation, medians (interquartile range IQR), and number (percentage) were used to depict normally distributed data, non-normally distributed continuous data, and categorical data, respectively. According to the application's requirements, the toxicity observation scale data were compared using Pearson's chi-square test. Other recorded data were compared using Student's t-test for categorical variables or the Mann–Whitney U test for quantitative variables. IBM SPSS Statistics for Windows (version 25.0, IBM Corp; Armony, NY) was used to analyze all data. All statistical tests were two-tailed, and $p < 0.05$ was considered statistically significant.
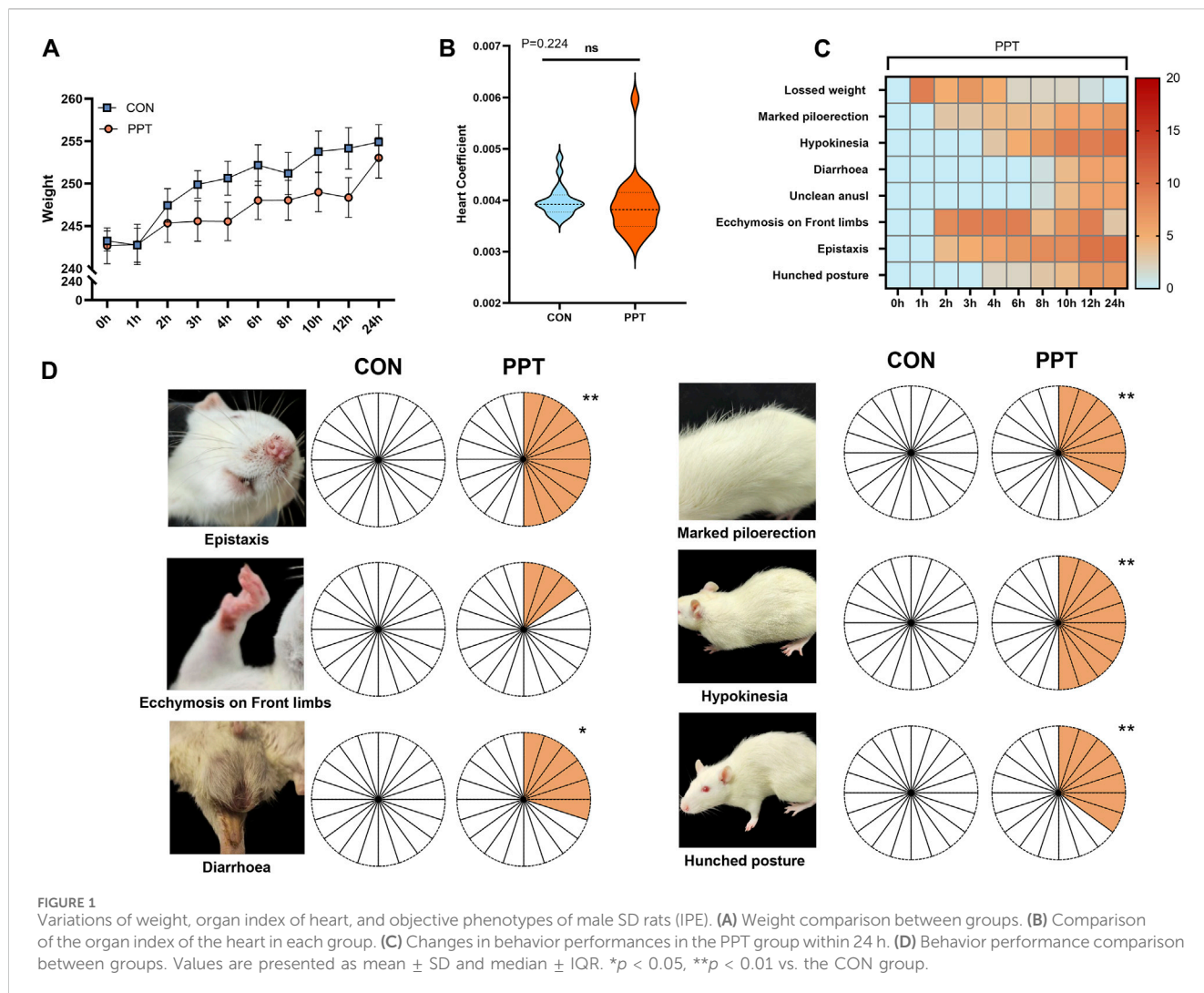
3 Results

3.1 Evaluation of cardiotoxicity induced by PPT (IPE and AOE)

3.1.1 Acute cardiotoxicity induced by PPT

Statistical analysis of rat weight showed that the weight of animals in the CON and PPT groups significantly increased after administration ($p < 0.05$). Compared with the CON group, the weight difference in rats in the PPT group before and after 24 h of administration was not statistically significant ($p > 0.05$) (Figure 1A. The statistical analysis of the organ index of the heart showed no statistically significant difference between the PPT and CON groups ($p > 0.05$) (Figure 1B and Supplementary Table S3). Behavior observation showed no significant changes in the CON group. Compared with the CON group, rats in the PPT group exhibited varying degrees of upright and rough hair, lazy movement, unclean anus, and oronasal hemorrhage. An obvious ecchymosis on the feet ($p < 0.01$) after 2 h of administration, obvious symptoms of oronasal hemorrhage ($p < 0.05$) after 3 h of administration, lazy movement ($p < 0.05$) after 6 h of administration, symptoms of upright and rough hair ($p < 0.05$) after 10 h of administration, and arched back ($p < 0.01$) after 12 h of administration (Figures 1C, D and Supplementary Table S1) were noted in rats of the PPT group.

3.1.2 Serum myocardial zymogram indicators

CK, CK-MB, LDH, AST, and α-HBD, commonly used indicators reflecting the degree of myocardial cell damage (Xuan and Jian, 2016), were assessed to evaluate the degree of cardiac damage caused by PPT. The results of serum biochemical parameters are shown in Figure 2A. Compared with the CON group, the levels of CK in the serum of rats in the PPT group were significantly reduced ($p < 0.01$), while those of CK-MB were significantly increased ($p < 0.01$); the levels of LDH, AST, and α-HBD showed an upward trend but without statistically significant differences ($p > 0.05$). These results indicated that after 24 h of gavage of the PPT aqueous solution to rats, serum myocardial enzyme concentrations fluctuated, with the most significant increase in CK-MB and decrease in CK levels.

FIGURE 1
Variations of weight, organ index of heart, and objective phenotypes of male SD rats (IPE). **(A)** Weight comparison between groups. **(B)** Comparison of the organ index of the heart in each group. **(C)** Changes in behavior performances in the PPT group within 24 h. **(D)** Behavior performance comparison between groups. Values are presented as mean $\pm$ SD and median $\pm$ IQR. *$p < 0.05$, **$p < 0.01$ vs. the CON group.

3.1.3 Cardiac injury markers

BNP, cTnI, Mb, and NT-proBNP levels are mainly used to diagnose symptoms of heart failure and myocardial infarction in clinical medicine (Kang et al., 2017). We evaluated cardiac injury by detecting the concentrations of BNP, cTnI, Mb, and NT-proBNP in the serum. ELISA results showed that compared with the CON group, the levels of BNP, NT-proBNP, cTnI, and Mb in the serum of rats in the PPT group were significantly increased ($p < 0.05$), indicating that the heart tissue of rats was damaged after 24 h of administering the PPT aqueous solution (Figure 2B).
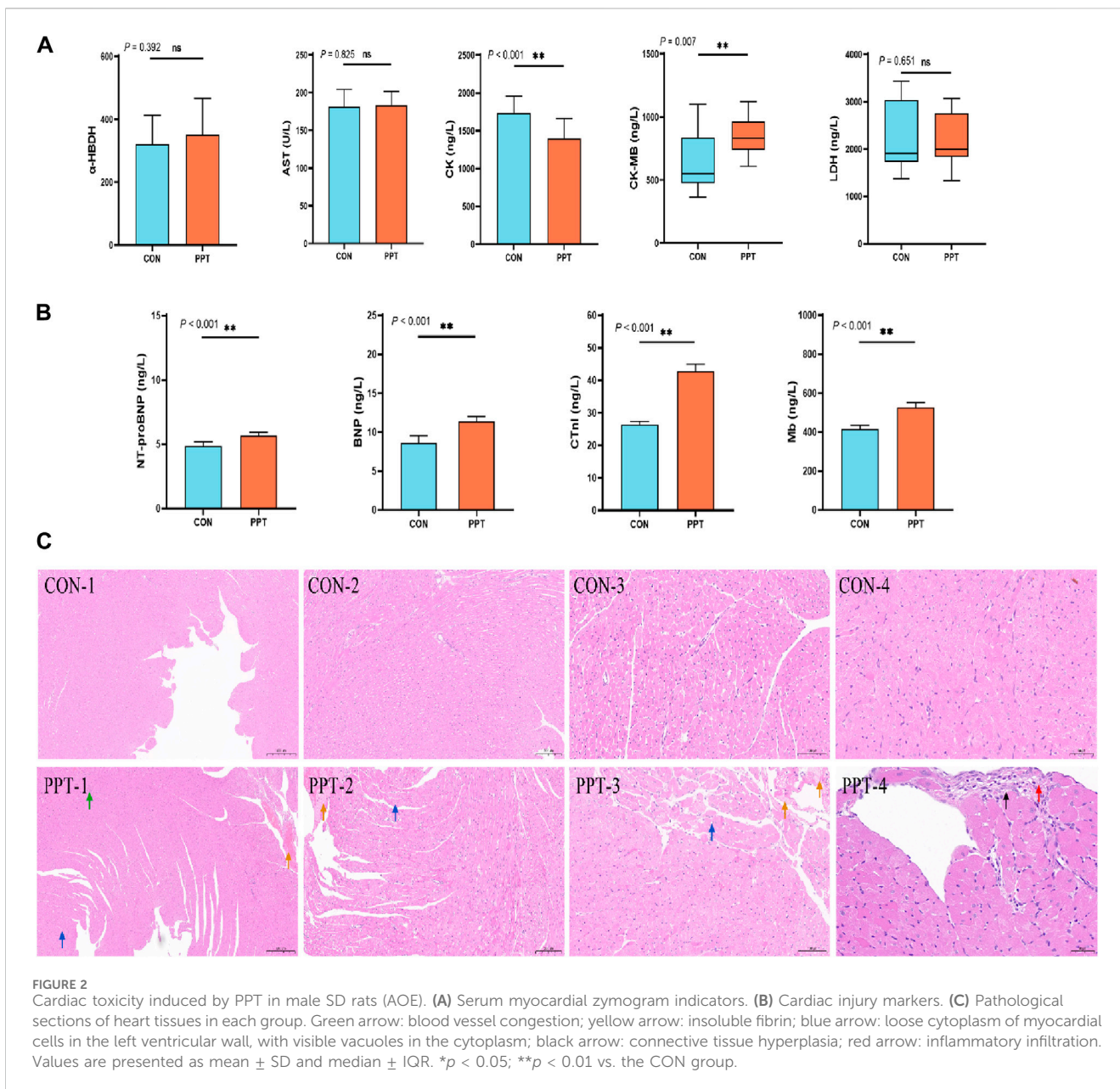
3.1.4 Pathological manifestations

Pathological manifestations of the rat hearts were observed under an optical microscope. Histopathological results showed that the heart tissue's endocardial and epicardia structures were clearly visible, the vascular structure was intact, the myocardial fibers were tightly arranged, the cell boundaries were clearly visible, and the cell morphology was consistent with no expansion, atrophy, degeneration, necrosis, or inflammatory cell infiltration in the CON group. Compared with the CON group, the PPT group showed a certain degree of cardiac damage, mainly manifested as vascular congestion, focal connective tissue hyperplasia, inflammatory

infiltration, cytoplasmic looseness of myocardial cells, and visible vacuoles in the cytoplasm. According to the International Harmonization of Nomenclature and Diagnostic Criteria for Lesions in Rats and Mice (INHAND) proposal (www.goReni.org.), the cardiac tissue of rats in the CON group was scored grade 0 and considered normal. The pathological rating of heart tissue in the PPT group was grade 1, and the pathological changes exceeded the normal range. Therefore, administration of the PPT aqueous solution caused some damage to the heart. The specific details are shown in Figure 2C. The pathological scoring criteria are shown in Supplementary Table S4.

3.2 Transcriptome analysis

A total of 92 DEGs, including 50 upregulated and 42 downregulated genes, were identified between the CON and PPT groups (Figure 3A). Cluster analysis of DEGs divided the CON group and PPT groups distinctly (Figure 3B). To determine the main biological functions related to DEGs, GO enrichment analysis was conducted (Figure 3C). Exposure to 120 mg/kg PPT primarily induced alterations in acute inflammatory responses, toxin metabolism, exogenous metabolism, positive regulation of mast cell activation,

FIGURE 2
Cardiac toxicity induced by PPT in male SD rats (AOE). **(A)** Serum myocardial zymogram indicators. **(B)** Cardiac injury markers. **(C)** Pathological sections of heart tissues in each group. Green arrow: blood vessel congestion; yellow arrow: insoluble fibrin; blue arrow: loose cytoplasm of myocardial cells in the left ventricular wall, with visible vacuoles in the cytoplasm; black arrow: connective tissue hyperplasia; red arrow: inflammatory infiltration. Values are presented as mean $\pm$ SD and median $\pm$ IQR. *$p < 0.05$; **$p < 0.01$ vs. the CON group.

and immune response regulatory signaling pathways. In terms of biological processes (BP), DEGs were mainly enriched in 4-nitrophenol metabolism, toxin metabolism, xenobiotic metabolic process, and positive regulation of mast cell activation. In terms of molecular functions (MF), DEGs were mainly enriched in oxidoreductase activity, MHC protein complex binding, intracellular sodium-activated potassium channel activity, and acetyl CoA activity. In terms of cellular components (CC), DEGs were mainly enriched in the synaptic vesicle lumen, voltage-gated sodium channel complex, dense core granule lumen, and sodium channel complex. Notably, to determine the potential enriched pathways related to DEGs, KEGG pathway enrichment analysis was performed for the 92 DEGs, with the results shown in Figures 3D, E. The primary altered metabolic or signaling pathways included arachidonic acid metabolism, linoleic acid metabolism, glycolysis, pentose phosphate pathway, amino acid

metabolism, phospholipase D signaling pathway, and the Notch signaling pathway.

3.3 Arachidonic acid metabolism disorder due to PPT-induced cardiotoxicity

3.3.1 Methodological investigation

The experimental methodology is shown in Supplementary Figure S1 and Supplementary Table S2, with the method repeatability and the sample stability meeting all requirements for metabolomics analysis (RSD (peak area) < 30%). The linear equations for all metabolites reached $r > 0.999$, and the chromatographic separation of each metabolite was good, with sharp and symmetrical peak shapes.
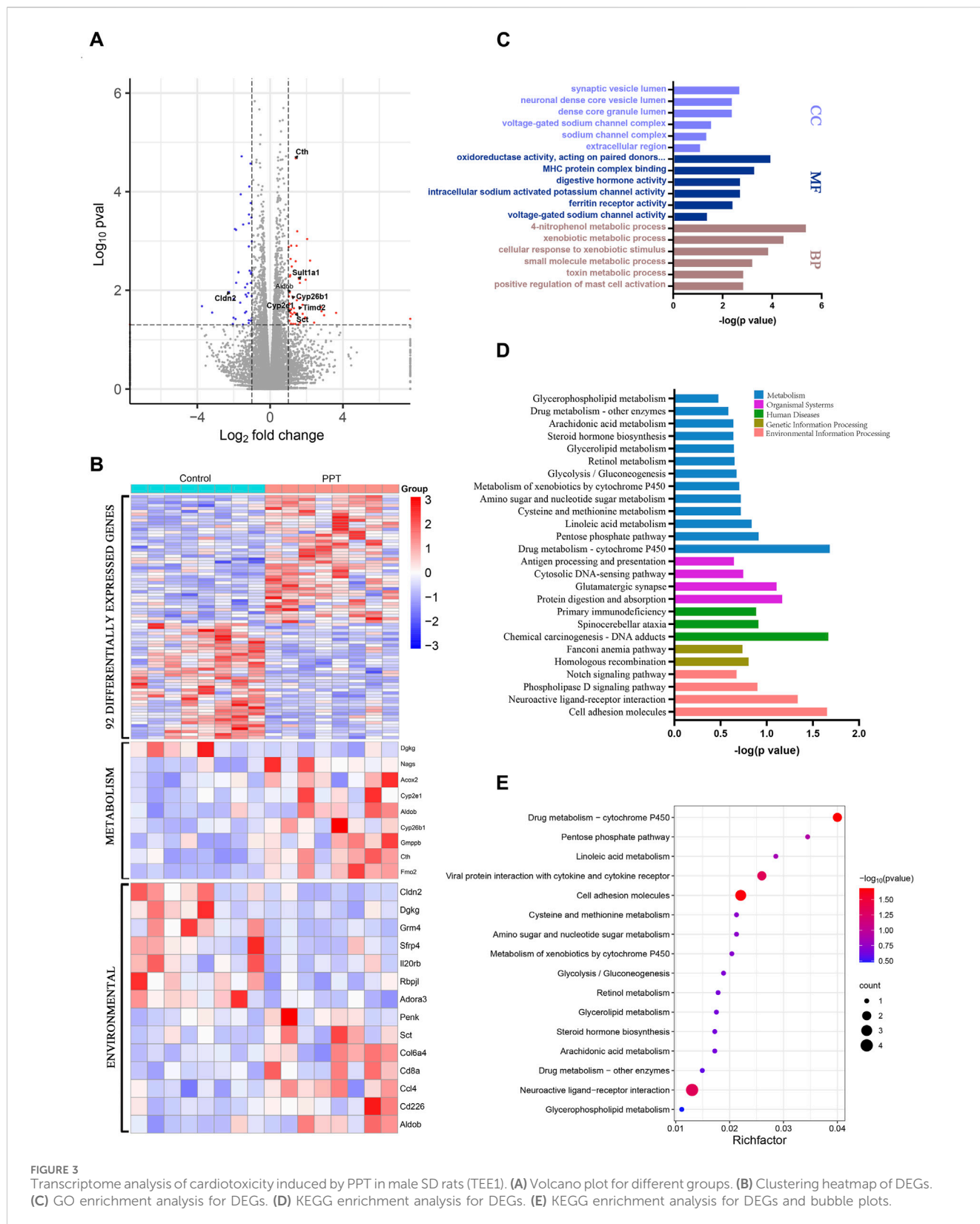
FIGURE 3
Transcriptome analysis of cardiotoxicity induced by PPT in male SD rats (TEE1). **(A)** Volcano plot for different groups. **(B)** Clustering heatmap of DEGs. **(C)** GO enrichment analysis for DEGs. **(D)** KEGG enrichment analysis for DEGs. **(E)** KEGG enrichment analysis for DEGs and bubble plots.

3.3.2 Metabolic profiling

Quantitative analysis was conducted on the 15 metabolites of the arachidonic acid pathway; except for leukotriene D4, which was not detected below the detection limit, the levels of the remaining 14 metabolites were measured in the PPT and CON groups (Table 2; Figure 4D). To distinguish the metabolic profiles among the CON and PPT groups, OPLS-DA in ESI⁻ mode (negative ion mode) was performed for cluster analysis. Significant separation of the CON

TABLE 2 Quantitative detection results of arachidonic acid targeted metabolomics ($\bar{x} \pm$ SD, M (IQR)).

Component name	Fold change	p	PPT	CON
Docosahexaenoic acid	2.520	0.020	68103.368 ± 42758.492	27026.253 ± 10888.772
Prostaglandin F2alpha	2.580	0.272	1.337 (4.25)	0.431 (0.99)
8-iso-Prostaglandin F2alpha	2.800	0.328	107.961 (696.87)	61.201 (108.27)
12(S)-HETE	3.549	0.407	12.127 (10.16)	9.095 (1.62)
Thromboxane B2	3.538	0.407	6.779 (3.04)	6.339 (0.72)
Leukotriene B4	1.321	0.456	23.499 (10.33)	20.821 (4.79)
Prostaglandin D2	1.337	0.461	8.195 (0.31)	8.12 (0.43)
14 (15)-EpETE	0.989	0.528	8.140 ± 0.251	8.230 ± 0.304
13(S)-HODE	0.789	0.691	108099.432 (62053.14)	105866.389 (34865.62)
Arachidonic acid	1.059	0.734	110328.950 ± 45779.398	104170.482 ± 20686.505
6-keto-Prostaglandin F1alpha	1.280	0.773	129.055 (183.59)	111.987 (57.94)
15(S)-HETE	1.149	0.822	38.822 (2.67)	38.566 (4.2)
Prostaglandin E2	0.986	0.840	103.414 (111.9)	133.963 (66.07)
9(S)-HODE	0.959	0.862	126.553 ± 78.072	132.019 ± 39.093

and PPT groups in OPLS-DA confirmed the reliability and reproducibility of the test method (Figures 4A, B). Furthermore, the permutation plot of PLS-DA showed that the model had no overfitting and was reliable (Figure 4C). Eight differential metabolites with $p <$ 0.05 and FC > 1.5 were selected as differential metabolites, including 12(S)-HETE, 8-iso-PGF$_{2\alpha}$, TXB2, 6-keto-PGF$_{1\alpha}$, 15(S)-HETE, DHA, PGD$_2$, and LTB$_4$. Compared with the CON group, all eight metabolites were upregulated after administration of PPT (Figures 4D, E).

3.4 Integrated analysis of genes, metabolites, myocardial enzymes, and cardiac injury markers

Correlation analysis was performed to assess the inter-relationships among genes, metabolites, myocardial enzymes, and cardiac injury markers. As shown in Figure 5, Cyp2e1 was positively correlated with several differential metabolites, including 8-iso-PGF2α, 12(S)-HETE, TXB2, LTB4, PGD2, and 6-keto-PGF1α. Aldob was positively correlated with 8-iso-PGF2α, 12(S)-HETE, TXB2, and PGD2. DHA, a differential metabolite, was positively correlated with differential genes Fmo2 and Timd2, as well as heart injury markers BNP and Mb.

4 Discussion

4.1 Toxicological research on cardiotoxicity induced by PPT (IPE and AOE)

In our previous work, we demonstrated that administering 1.2 g/kg/day of DV to SD rats induced toxicity (Liu et al., 2020). For the clinical context, the commonly prescribed dosage range for DV is 3–9 g for a 60-kg adult human, equivalent to an experimental dose of approximately 0.6 g/kg/day for rats when adjusted for the

body surface area (Xu et al., 2002). Given that the PPT content in DV is 91 mg/g (Wang et al., 2017), the experimental dose for this study was calculated as 109 mg kg−1 (1.2 × 91 = 109.2 mg kg−1), which is roughly double the clinically relevant dose. Therefore, we selected 120 mg/kg to robustly evaluate the potential cardiotoxicity effects of PPT. This study revealed for the first time that rats in the PPT group exhibited symptoms of diarrhea, marked piloerection, epistaxis (nosebleeds), hunched posture, and hypokinesia (reduced movement), which intensified over time within 24 h after administration of 120 mg/kg PPT. Interestingly, we report for the first time that the symptoms of ecchymosis (bruising) in the PPT group rats decreased within 24 h after administration. Although the body weight of the PPT group rats was significantly lower than that of the CON group between 2 and 12 h after administration, there was no significant difference in body weight between the two groups by 24 h. We speculate that the above situation may be because the rats may have triggered a self-repair or regulatory process in the first 24 h of exposure to PPT, especially between 13 h and 24 h. In this study, the body weight of the rats increased significantly within 24 h, and even that in the CON group rats increased by nearly 10 g within 24 h. This may be because we used 7-week-old SD rats in a rapid growth stage of sexual maturity which were made to fast, and water access was prevented for 8 h before administration. The rats were made to fast, and water access was prevented 1 h after administration. After providing sufficient food and water 1 h after administration, the body weight of the rats increased significantly within 24 h.

There was a statistically significant decrease in CK content ($p < 0.05$) and a remarkable increase in CK-MB content ($p < 0.05$) in the PPT group compared to the CON group. This pattern of change suggests possible myocardial injury in the experimental rats, as CK-MB is a more specific marker of cardiac muscle damage than CK. This unequal expression suggests that SD rats may be in the early stage of myocardial injury, as CK-MB
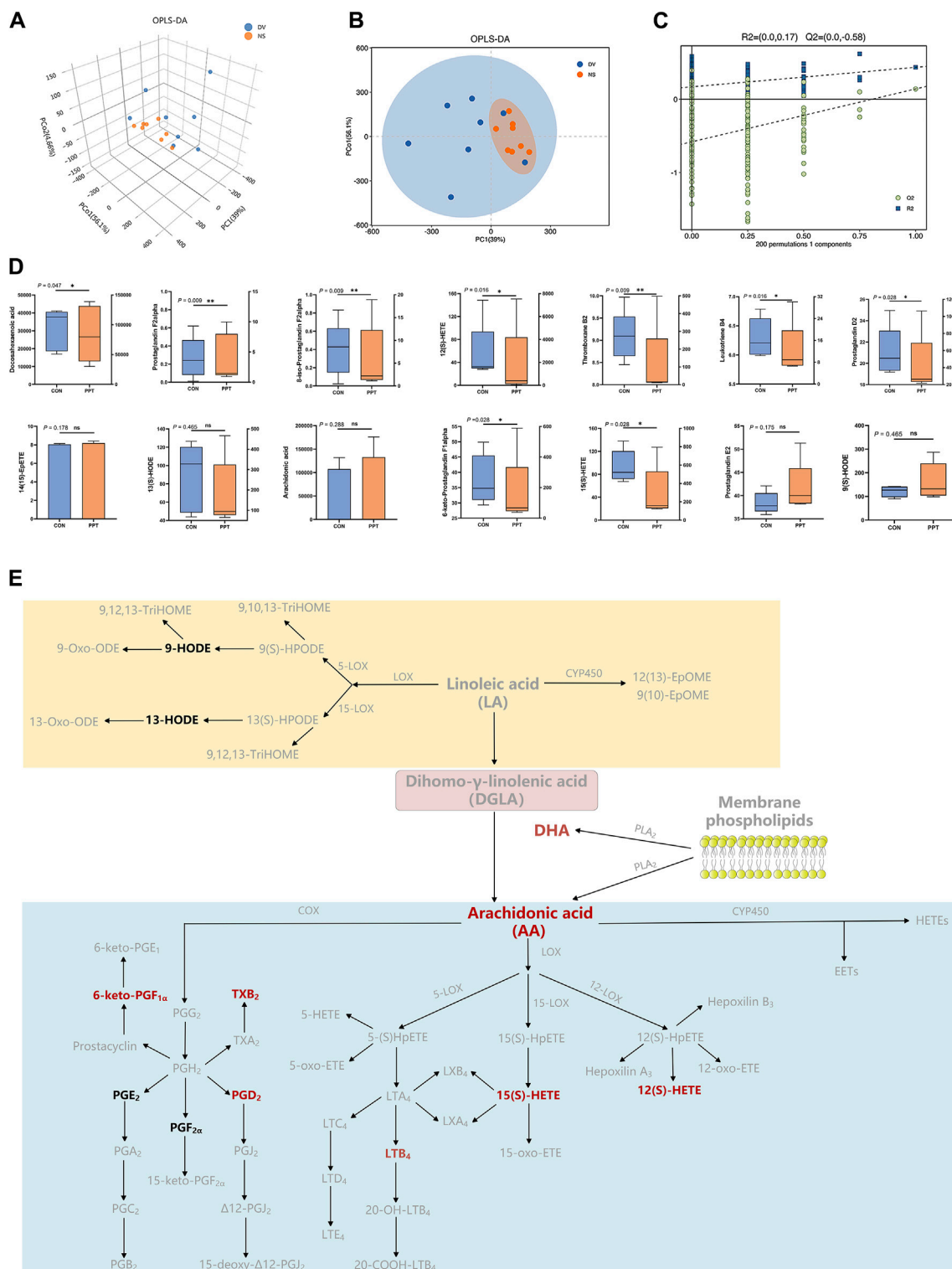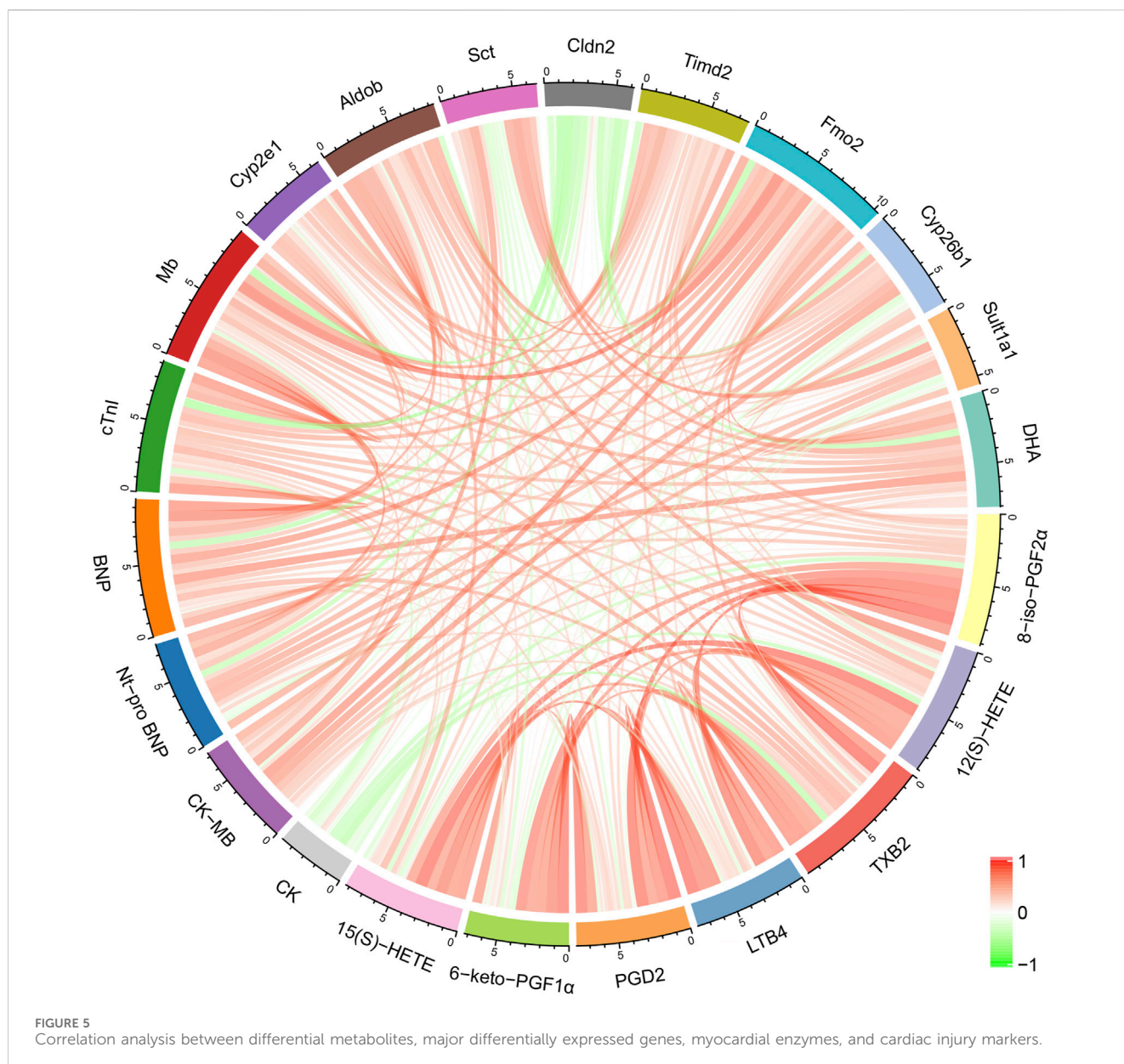
FIGURE 4
Targeted metabolomics analysis of PPT-induced cardiotoxicity in male SD rats (TEE2). **(A)** OPLS-DA 3D score plots in ESI⁻ mode. **(B)** OPLS-DA score plots in ESI⁻ mode. **(C)** Permutation test for OPLS-DA in ESI⁻ mode. **(D)** Quantitative results of arachidonic acid metabolites in different groups. **(E)** Differential metabolites of arachidonic acid metabolic pathways; potential metabolites in red and other metabolites in black. Data presented as mean $\pm$ SD and median $\pm$ IQR. *$p < 0.05$, **$p < 0.01$ vs. the CON group.

FIGURE 5
Correlation analysis between differential metabolites, major differentially expressed genes, myocardial enzymes, and cardiac injury markers.

is mainly present in cardiac muscle cells. Its elevation is usually more sensitive than CK—when myocardial injury is in the early stage, only a small portion of B subunits are released into peripheral blood due to the presence of M subunits in myocardial cells, and CK produced by other cells in the body is absorbed by surplus CK-MB, resulting in a decrease in CK levels (Bertinchant et al., 2000; Ma et al., 2023). In clinical settings, the increase in BNP levels is the specific gold standard for diagnosing cardiac dysfunction. BNP is synthesized and secreted by ventricular muscle cells, and its level can increase 200–300 times when myocardial infarction—cardiac overload—or dilation occurs (McGrath et al., 2005; Sun et al., 2023). CTnI and Mb mainly exist in the myocardium and can be detected in the serum 2 h after cardiac damage (Apple, 1999; Kyriazidis et al., 2023). These characteristics enable BNP, cTnI, and Mb to serve as more sensitive indicators of cardiac damage. These results indicate that PPT may cause a certain degree of

damage to the rats' hearts. To further evaluate the cardiotoxicity due to PPT, we conducted pathological observations on the heart tissues of rats after administering PPT intragastrically. The PPT group showed a certain degree of cardiac damage. According to the degree of pathological changes in heart tissue, INHAND was used to stratify the histopathological results into five grades: 0, 1, 2, 3, and 4. As the grade ascends, the corresponding degree of tissue damage progressively intensifies. Grade 0 signifies that the tissue alterations remain within normal limits, whereas grade 1 indicates that the tissue changes surpassed the normal range. Grade 4, on the other hand, denotes that the lesions have encompassed the entire tissue or organs. In this study, the pathological assessment of heart tissue from rats in the PPT group was classified as grade 1, suggesting that PPT induced notable morphological alterations in the rat heart tissue. In summary, administering 120 mg/kg PPT within 24 h may cause cardiac injury.

4.2 Mechanism underlying acute cardiac toxicity induced by PPT in rats

In this study, transcriptomics was employed to characterize the gene expression in rats following PPT administration. PPT disrupted the genetic equilibrium in rats, resulting in significant alterations in 92 genes, with 50 genes being upregulated and 42 downregulated. GO analysis showed that these genes were mainly involved in biological processes, such as oxidoreductase activity, toxin metabolism, 4-nitrophenol metabolic process, and synaptic vesicle lumen. Pathway enrichment analysis for DEGs revealed a significant involvement in arachidonic acid metabolism, linoleic acid metabolism, glycolysis, pentose phosphate pathway, amino acid metabolism, phospholipase D signaling pathway, and the Notch signaling pathway. Arachidonic acid metabolism, linoleic acid metabolism, phospholipase D signaling pathway, and Notch signaling pathway are closely related to inflammation. Glycolysis and pentose phosphate pathways are involved in the energy metabolism of the heart. Therefore, PPT may lead to cardiac energy metabolism disorders and inflammation by altering related genes/proteins. To verify this hypothesis, targeted metabolomic technology was used in this study to characterize the arachidonic acid metabolic profile involved in the inflammatory response. Among the 14 detected metabolites, eight differential metabolites were upregulated, including: DHA, AA, and their metabolite; LTB4, PGD2, and 8-iso-PGF2α; TXB2, 12(S)-HETE, and 15(S)-HETE. The main differential metabolites are closely related to the occurrence, development, and resolution of inflammation, which play a crucial role in the development and progression of cardiovascular disease. LTB4, the pro-inflammatory lipid mediator produced by the metabolism of LOXs (Lipoxygenases), increases vascular permeability by activating the CysLT2 receptor in blood vessels, mediating myocardial ischemia and reperfusion injury (Jiang et al., 2008). 12-HETE is produced primarily by the 12-LOX, which exerts a chemotaxis effect that promotes the exudation, adhesion, and aggregation of leukocytes. 12-HETE contributes to sustained inflammation and increased cardiomyocyte death, elevating pro-inflammatory markers such as MCP-1 and IL-6 and resulting in monocyte and neutrophil recruitment during the acute phase post-MI (Kuzuya et al., 1987; Shibata et al., 1988). 12-HETE is involved in oxidative stress. It promotes ROS generation, which activates the transcription factor NF-κB and regulates the expression of many genes. 12 HETE significantly increases the levels of phosphorylated NF-κB, which in turn leads to β cell dysfunction (Weaver et al., 2012). Inflammatory reactions and massive PG levels are induced in the heart tissues after ischemic conditions (Kong et al., 2016; Tang et al., 2017) or DOX treatment (Robison and Giri, 1987). Similarly, in our study, the level of PGD2, a COX-derived AA metabolite, in the PPT rats was remarkably higher than that in the CON group. Cardiac-generated prostanoids, particularly PGD2, directly mediate cardiac myocyte apoptosis after myocardial ischemia (Qiu et al., 2012).

Through integrated analysis, we observed that Cyp2e1 was positively correlated with a series of differential metabolites, including 8-iso-PGF2α, 12(S)-HETE, TXB2, LTB4, PGD2, and 6-keto-PGF1α. Cyp2e1 (cytochrome P450 2E1) overexpression can increase the necrosis and apoptosis of cardiomyocytes (Zhang et al., 2011). Cyp2e1 can promote injury in diabetic heart microvascular

endothelial cells by increasing the production of ROS under high glucose conditions, and quercetin can reduce the damage caused by high sugar-induced cardiac microvascular endothelial cells by inhibiting Cyp2e1 (Chen et al., 2018). The expression of Cyp2e1 increases in alcoholic cardiomyopathy, which mediates the transformation of cardiac fibroblasts into myofibroblasts, leading to myocardial fibrosis (Zhang et al., 2023). Aldob is significantly positively correlated with 8-iso-PGF2α, 12(S)-HETE, TXB2, and PGD2. Fructose-bisphosphate aldolase B (Aldob) is a tetrameric glycolytic enzyme mainly involved in synthesizing D-glyceraldehyde 3-phosphate and glycerone phosphate from D-glucose as part of the glycolysis and carbohydrate degradation pathways. As one of the indicators of the CS4P score, ALDOB is not cardiac-specific but reflects multiorgan dysfunction, systemic inflammation, and immune activation (Iborra-Egea et al., 2020a; Iborra-Egea et al., 2020b). DHA has anti-inflammatory effects, producing anti-inflammatory and inflammation-resolving mediators such as resolvins, protectins, and maresins (omega-3 fatty acids and inflammatory processes from molecules to man). DHA was positively correlated with the differential gene Fmo2 (flavin-containing monooxygenase 2), as well as the heart injury markers BNP and Mb. The expression of FMO2 in the heart is primarily enriched in fibroblasts rather than myocytes. Fmo2 can prevent cardiac fibrosis. A significant downregulation of FMO2 is consistently observed in hearts after myocardial infarction (MI) in rodents. In this study, after exposure to PPT, both anti-inflammatory DHA and fibrosis-inhibiting Fmo2 were upregulated, suggesting that the heart is fighting against the interference of PPT to maintain homeostasis.

Collectively, the mechanism of PPT-induced acute cardiotoxicity involves oxidative stress, apoptosis, inflammatory response, and disorder of the energy metabolism.

4.3 Limitations

The objective of this study was to confirm acute cardiotoxicity induced by PPT in male SD rats within 24 h and to investigate the underlying mechanisms. However, due to euthanasia and sampling of all experimental animals 24 h post-administration, continuous observation was not feasible, making it impossible to ascertain the reversibility of the observed IPE phenotype. The dosage employed in this study was based on clinical application and prior studies, with a single dose administered without exploring the dose–response relationship. Future studies should encompass a range of doses to gain a more comprehensive understanding. Furthermore, while this study utilized transcriptomics to detect expressional changes across the entire transcriptome, the lack of quantitative analysis (qRT-PCR) precluded in-depth expression intensity analysis. Moreover, functional validation has not been performed on the identified key genes or differential metabolites. As such, future research should aim to silence critical genes at the cellular level using RNAi technology or inhibit them with corresponding inhibitors. Similarly, inhibitors or gene-knockout technology can be employed at the whole animal level to verify their impact on the onset and progression of PPT-induced cardiac toxicity. By manipulating the levels of differential metabolites, toxicological

FIGURE 6
Full-text summary diagram.
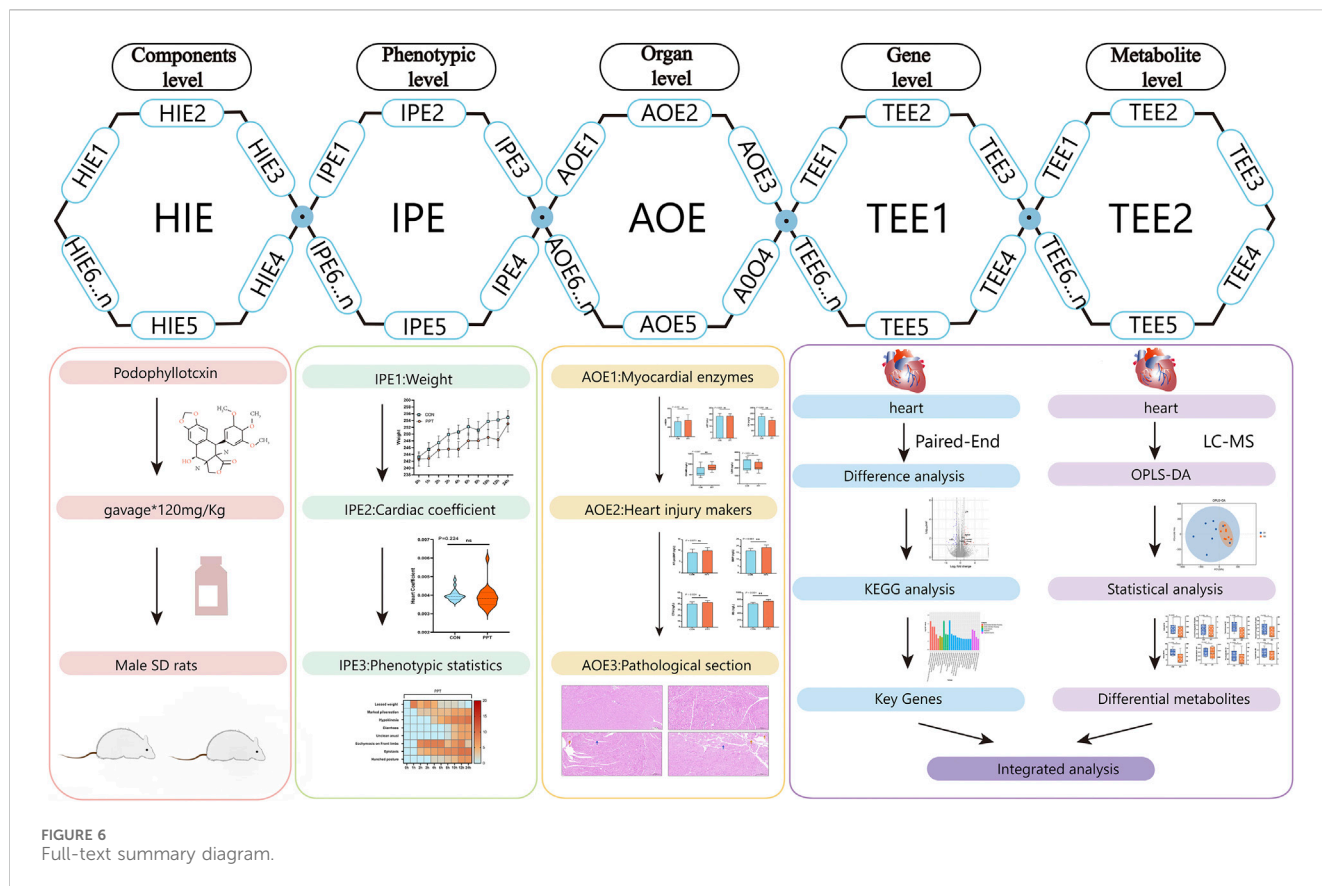
alterations in animals can be observed and potential biomarkers and therapeutic drugs can be uncovered.

5 Conclusion

The results of this study provide a preliminary understanding of the molecular mechanisms of cardiotoxicity caused by PPT. Injury phenotypic changes were assessed based on alterations in body weight, behavioral changes (IPE). Adverse outcomes evidence was evaluated through elevations in myocardial enzymes and cardiac injury biomarkers, along with histopathological observations (AOE). Furthermore, the study illustrated transcriptome characteristics and arachidonic acid metabolism profiles (TEE). Finally, the mechanism of acute cardiotoxicity caused by PPT involves oxidative stress, apoptosis, inflammatory response, and disordered energy metabolism. The developed TEC concept can serve as a useful tool to integrate data from multi-platform systems biology techniques, with the potential of broad-ranging application to other herbal medicines to determine new indicators of organ injury and toxicant studies to analyze omics data and identify the mechanisms underlying toxicity (Figure 6).

Data availability statement

All raw reads data were stored in the NCBI sequence read archive (SRA accession number: PRJNA1154551).

Ethics statement

The animal study was approved by Animal Ethics Committee of Beijing University of Traditional Chinese Medicine (BUCM-2023042701-2049). The study was conducted in accordance with the local legislation and institutional requirements.

Author contributions

KM: data curation, investigation, methodology, project administration, writing–original draft, and writing–review and editing. LS: software, visualization, writing–original draft, and writing–review and editing. CJ: data curation, investigation, methodology, and writing–review and editing. HK: investigation, methodology, and writing–review and editing. JX: investigation, methodology, and writing–review and editing. SZ: investigation, methodology, and writing–review and editing. SH: software, visualization, and writing–review and editing. JQ: methodology and writing–review and editing. CL: conceptualization, funding acquisition, supervision, and writing–review and editing. JH: resources, supervision, validation, and writing–review and editing.

Funding

Conflict of interest

The authors declare that the research was conducted in the absence of any commercial or financial relationships that could be construed as a potential conflict of interest.

Publisher's note

All claims expressed in this article are solely those of the authors and do not necessarily represent those of their affiliated organizations, or those of the publisher, the editors, and the reviewers. Any product that may be evaluated in this article, or claim that may be made by its manufacturer, is not guaranteed or endorsed by the publisher.

Supplementary material

The Supplementary Material for this article can be found online at: https://www.frontiersin.org/articles/10.3389/fphar.2024.1378758/full#supplementary-material

References

Althurwi, H. N., Tse, M. M. Y., Abdelhamid, G., Zordoky, B. N. M., Hammock, B. D., and El-Kadi, A. O. S. (2013). Soluble epoxide hydrolase inhibitor, TUPS, protects against isoprenaline-induced cardiac hypertrophy. *Br. J. Pharmacol.* 168, 1794–1807. doi:10.1111/bph.12066

Amara, I. E. A., Elshenawy, O. H., Abdelrady, M., and El-Kadi, A. O. S. (2014). Acute mercury toxicity modulates cytochrome P450, soluble epoxide hydrolase and their associated arachidonic acid metabolites in C57Bl/6 mouse heart. *Toxicol. Lett.* 226, 53–62. doi:10.1016/j.toxlet.2014.01.025

Apple, F. S. (1999). Tissue specificity of cardiac troponin I, cardiac troponin T and creatine kinase-MB. *Clin. Chim. Acta Int. J. Clin. Chem.* 284, 151–159. doi:10.1016/s0009-8981(99)00077-7

Auchampach, J. A., Ge, Z.-D., Wan, T. C., Moore, J., and Gross, G. J. (2003). A3 adenosine receptor agonist IB-MECA reduces myocardial ischemia-reperfusion injury in dogs. *Am. J. Physiol. Heart CircPhysiol* 285, H607–H613. doi:10.1152/ajpheart.01001.2002

Bellien, J., and Joannides, R. (2013). Epoxyeicosatrienoic acid pathway in human health and diseases. *J. Cardiovasc. Pharmacol.* 61, 188–196. doi:10.1097/FJC.0b013e318273b007

Bertinchant, J. P., Robert, E., Polge, A., Marty-Double, C., Fabbro-Peray, P., Poirey, S., et al. (2000). Comparison of the diagnostic value of cardiac troponin I and T determinations for detecting early myocardial damage and the relationship with histological findings after isoprenaline-induced cardiac injury in rats. *Clin. Chim. Acta Int. J. Clin. Chem.* 298, 13–28. doi:10.1016/s0009-8981(00)00223-0

Borea, P. A., Gessi, S., Bar-Yehuda, S., and Fishman, P. (2009). A3 adenosine receptor: pharmacology and role in disease. *HandbExpPharmacol*, 297–327. doi:10.1007/978-3-540-89615-9_10

Cao, F., Deng, C., and Zhou, M. (2011). One case of multiple organ failure caused by medicinal wine poisoning of DysosmaVersipellis. *J. Clin. Emerg.* 12, 62–63.

Chen, S., Feng, J., Qiu, S., Hou, J., Shen, Y., Yang, C., et al. (2018). Quercetin attenuates the high glucose-induced damage of mouse cardiac microvascular endothelial cells via inhibiting CYP2E1. *Journalof Clin. Cardiol.* 34, 722–726. doi:10.13201/j.issn.1001-1439.2018.07.021

Chinese national standard GB/T 21757-2008 (2008). Chemicals-Test method of acute oral toxicity for chemicals-Acute toxic class method. Available at: (in Chinese) https://std.samr.gov.cn/search/std?q=GB%2FT%2021757-2008.

Duan, J., Sun, J., Jiang, T., Ma, X., Li, X., Wang, Y., et al. (2024). Podophyllotoxin-mediated neurotoxicity via the microbiota-gut-brain axis in SD rats based on the toxicological evidence chain (TEC) concept. *Sci. Total Environ.* 907, 168106. doi:10.1016/j.scitotenv.2023.168106

Ganapathy, A. S., Saha, K., Suchanec, E., Singh, V., Verma, A., Yochum, G., et al. (2022). AP2M1 mediates autophagy-induced CLDN2 (claudin 2) degradation through endocytosis and interaction with LC3 and reduces intestinal epithelial tight junction permeability. *Autophagy* 18, 2086–2103. doi:10.1080/15548627.2021.2016233

Gao, S., Yu, J., Gao, J. Y., Gao, J., Li, Z., Zhang, H., et al.(2016). Incorrect administration of podophyllum Chinese herbs and clinical treatment of related poisoning. *Henan Tradit. Chin. Med.* 36, 161–162. doi:10.16367/j.issn.1003-5028.2016.01.0070

Gu, Y., Zhou, Y., Ju, S., Liu, X., Zhang, Z., Guo, J., et al. (2022). Multi-omics profiling visualizes dynamics of cardiac development and functions. *Cell Rep.* 41, 111891. doi:10.1016/j.celrep.2022.111891

Hartman, J. H., Miller, G. P., and Meyer, J. N. (2017). Toxicological implications of mitochondrial localization of CYP2E1. *Toxicol. Res. (Camb)* 6, 273–289. doi:10.1039/C7TX00020K

Headrick, J. P., and Peart, J. (2005). A3 adenosine receptor-mediated protection of the ischemic heart. *VasculPharmacol* 42, 271–279. doi:10.1016/j.vph.2005.02.009

Huang, G., Huang, Z., Peng, Y., Wang, Y., Liu, W., Xue, Y., et al. (2021). Metabolic processes are potential biological processes distinguishing nonischemic dilated cardiomyopathy from ischemic cardiomyopathy: a clue from serum proteomics. *PharmgenomicsPers Med.* 14, 1169–1184. doi:10.2147/PGPM.S323379

Iborra-Egea, O., Montero, S., and Bayes-Genis, A. (2020a). An outlook on biomarkers in cardiogenic shock. *CurrOpinCrit Care* 26, 392–397. doi:10.1097/MCC.0000000000000739

Iborra-Egea, O., Rueda, F., García-García, C., Borràs, E., Sabidó, E., and Bayes-Genis, A. (2020b). Molecular signature of cardiogenic shock. *Eur. Heart J.* 41, 3839–3848. doi:10.1093/eurheartj/ehz783

Jiang, W., Hall, S. R., Moos, M. P. W., Cao, R. Y., Ishii, S., Ogunyankin, K. O., et al. (2008). Endothelial cysteinyl leukotriene 2 receptor expression mediates myocardial ischemia-reperfusion injury. *Am. J. Pathol.* 172, 592–602. doi:10.2353/ajpath.2008.070834

Jin, Y. (1979). The role of unstable metabolites of arachidonic acid in hemostasis and thrombosis. *J. Med. Mol. Biol.* 284–288. doi:10.1093/oxfordjournals.bmb.a071482

Johansson, A., Curran, J. E., Johnson, M. P., Freed, K. A., Fenstad, M. H., Bjørge, L., et al. (2011). Identification of ACOX2 as a shared genetic risk factor for preeclampsia and cardiovascular disease. *Eur. J. Hum. Genet.* 19, 796–800. doi:10.1038/ejhg.2011.19

Kang, Q., Wan, Z., and Huang, Z. (2017). N-terminal probrain natriuretic peptide in patients with acute coronary syndrome. *Int. J. Clin. Pharmacol. Ther.* 55, 78–84. doi:10.5414/CP202632

Kong, D., Shen, Y., Liu, G., Zuo, S., Ji, Y., Lu, A., et al. (2016). PKA regulatory IIα subunit is essential for PGD2-mediated resolution of inflammation. *J. Exp. Med.* 213, 2209–2226. doi:10.1084/jem.20160459

Kong, J., He, T., Liu, C., and Huang, J. (2022). Multi modular toxicity assessment of nephrotoxicity in podophyllotoxin exposure rats on account of toxicological evidence chain (TEC) concept. *Ecotoxicol. Environ. Saf.* 231, 113157. doi:10.1016/j.ecoenv.2021.113157

Kong, J., Kui, H., Tian, Y., Kong, X., He, T., Li, Q., et al. (2023). Nephrotoxicity assessment of podophyllotoxin-induced rats by regulating PI3K/Akt/mTOR-Nrf2/HO1 pathway in view of toxicological evidence chain (TEC) concept. *Ecotoxicol. Environ. Saf.* 264, 115392. doi:10.1016/j.ecoenv.2023.115392

Kuzuya, T., Hoshida, S., Nishida, M., Kim, Y., Kamada, T., and Tada, M. (1987). Increased production of arachidonate metabolites in an occlusion-reperfusion model of canine myocardial infarction. *Cardiovasc. Res.* 21, 551–558. doi:10.1093/cvr/21.8.551

Kyriazidis, I. P., Jakob, D. A., Vargas, J. A. H., Franco, O. H., Degiannis, E., Dorn, P., et al. (2023). Accuracy of diagnostic tests in cardiac injury after blunt chest trauma: a systematic review and meta-analysis. *World J. Emerg. Surg. WJES* 18, 36. doi:10.1186/s13017-023-00504-9

Larabi, A., Barnich, N., and Nguyen, H. T. T. (2020). New insights into the interplay between autophagy, gut microbiota and inflammatory responses in IBD. *Autophagy* 16, 38–51. doi:10.1080/15548627.2019.1635384

Lee, S. H., Kim, N., Kim, M., Woo, S.-H., Han, I., Park, J., et al. (2022). Single-cell transcriptomics reveal cellular diversity of aortic valve and the immunomodulation by PPARγ during hyperlipidemia. *Nat. Commun.* 13, 5461. doi:10.1038/s41467-022-33202-2

Liu, C., Zhang, C., He, T., Sun, L., Wang, Q., Han, S., et al. (2020). Study on potential toxic material base and mechanisms of hepatotoxicity induced by Dysosmaversipellis

based on toxicological evidence chain (TEC) concept. *Ecotoxicol. Environ. Saf.* 190, 110073. doi:10.1016/j.ecoenv.2019.110073

Ma, Y., Wang, P., Wu, Z., Li, M., Gu, Y., Wu, H., et al. (2023). Curdione relieved isoproterenol-induced myocardial damage through inhibiting oxidative stress and apoptosis. *Am. J. Chin. Med.* 51, 73–89. doi:10.1142/S0192415X23500052

Ma, Z.-G., Yuan, Y.-P., Zhang, X., Xu, S.-C., Wang, S.-S., and Tang, Q.-Z. (2017). Piperine attenuates pathological cardiac fibrosis via PPAR-γ/AKT pathways. *EBioMedicine* 18, 179–187. doi:10.1016/j.ebiom.2017.03.021

Martin, S. A., Brash, A. R., and Murphy, R. C. (2016). The discovery and early structural studies of arachidonic acid. *J. Lipid Res.* 57, 1126–1132. doi:10.1194/jlr.R068072

Mawhin, M.-A., Tilly, P., Zirka, G., Charles, A.-L., Slimani, F., Vonesch, J.-L., et al. (2018). Neutrophils recruited by leukotriene B4 induce features of plaque destabilization during endotoxaemia. *Cardiovasc. Res.* 114, 1656–1666. doi:10.1093/cvr/cvy130

McGrath, M. F., de Bold, M. L. K., and de Bold, A. J. (2005). The endocrine function of the heart. *Trends Endocrinol. Metab. Tem.* 16, 469–477. doi:10.1016/j.tem.2005.10.007

Mustafa, S. J., Morrison, R. R., Teng, B., and Pelleg, A. (2009). Adenosine receptors and the heart: role in regulation of coronary blood flow and cardiac electrophysiology. *HandbExpPharmacol*, 161–188. doi:10.1007/978-3-540-89615-9_6

Nazarewicz, R. R., Zenebe, W. J., Parihar, A., Parihar, M. S., Vaccaro, M., Rink, C., et al. (2007). 12(S)-hydroperoxyeicosatetraenoic acid (12-HETE) increases mitochondrial nitric oxide by increasing intramitochondrialcalcium. *Arch. Biochem. Biophys.* 468, 114–120. doi:10.1016/j.abb.2007.09.018

Nishat, S., Khan, L. A., Ansari, Z. M., and Basir, S. F. (2016). Adenosine A3 Receptor: a promising therapeutic target in cardiovascular disease. *CurrCardiol Rev.* 12, 18–26. doi:10.2174/1573403x12666160111125116

Pathak, K., Pathak, M. P., Saikia, R., Gogoi, U., Sahariah, J. J., Zothantluanga, J. H., et al. (2022). Cancer chemotherapy via natural bioactive compounds. *Curr. Drug Discov. Technol.* 19, e310322202888. doi:10.2174/1570163819666220331095744

Qiu, H., Liu, J.-Y., Wei, D., Li, N., Yamoah, E. N., Hammock, B. D., et al. (2012). Cardiac-generatedprostanoids mediate cardiac myocyte apoptosis after myocardial ischaemia. *Cardiovasc. Res.* 95, 336–345. doi:10.1093/cvr/cvs191

Rand, A. A., Barnych, B., Morisseau, C., Cajka, T., Lee, K. S. S., Panigrahy, D., et al. (2017). Cyclooxygenase-derived proangiogenic metabolites of epoxyeicosatrienoic acids. *Proc. Natl. Acad. Sci. U. S. A.* 114, 4370–4375. doi:10.1073/pnas.1616893114

Robison, T. W., and Giri, S. N. (1987). Effects of chronic administration of doxorubicin on plasma levels of prostaglandins, thromboxane B2, and fatty acids in rats. *Cancer ChemotherPharmacol* 19, 213–220. doi:10.1007/BF00252975

Sacerdoti, D., Pesce, P., Di Pascoli, M., Brocco, S., Cecchetto, L., and Bolognesi, M. (2015). Arachidonic acid metabolites and endothelial dysfunction of portal hypertension. *Prostagl. Other Lipid Mediat* 120, 80–90. doi:10.1016/j.prostaglandins.2015.05.008

Sakariassen, K. S., Alberts, P., Fontana, P., Mann, J., Bounameaux, H., and Sorensen, A. S. (2009). Effect of pharmaceutical interventions targeting thromboxane receptors and thromboxane synthase in cardiovascular and renal diseases. *Future Cardiol.* 5, 479–493. doi:10.2217/fca.09.33

Schaefer, S., and Guerra, B. (2017). Protein kinase CK2 regulates redox homeostasis through NF-κB and Bcl-xL in cardiomyoblasts. *Mol. Cell Biochem.* 436, 137–150. doi:10.1007/s11010-017-3085-y

Shetty, G. A., Hattiangady, B., Upadhya, D., Bates, A., Attaluri, S., Shuai, B., et al. (2017). Chronic oxidative stress, mitochondrial dysfunction, Nrf2 activation and inflammation in the Hippocampus accompany heightened systemic inflammation and oxidative stress in an animal model of gulf war illness. *Front. Mol. Neurosci.* 10, 182. doi:10.3389/fnmol.2017.00182

Shibata, N., Akagami, H., Sanma, H., and Goshima, K. (1988). Augmentation of eicosanoids in ischemic heart muscle in dogs: its role in the deterioration of the ischemic lesion. *Jpn. Circ. J.* 52, 673–683. doi:10.1253/jcj.52.673

S, T., and P, P. (2014). Inside epoxyeicosatrienoic acids and cardiovascular disease. *Front. Pharmacol.* 5, 239. doi:10.3389/fphar.2014.00239

State Administration for Market Regulation and Standardization Administration (2008). Chemicals - test method of acute oral toxicity for chemicals - acute toxic class method GB/T 21757-2008. Available at: https://openstd.samr.gov.cn/bzgk/gb/newGbInfo?hcno=B34457D7CE6B4A1DFDD633B84FB62588 (Accessed January 8, 2024).

Sun, Y., Ma, M., Cao, D., Zheng, A., Zhang, Y., Su, Y., et al. (2023). Inhibition of fap promotes cardiac repair by stabilizing BNP. *Circ. Res.* 132, 586–600. doi:10.1161/CIRCRESAHA.122.320781

Tan, X.-M., Zhou, Y.-Q., Zhou, X.-L., Xia, X.-H., Wei, Y., He, L.-L., et al. (2018). Diversity and bioactive potential of culturable fungal endophytes of Dysosmaversipellis; a rare medicinal plant endemic to China. *Sci. Rep.* 8, 5929. doi:10.1038/s41598-018-24313-2

Tang, J., Shen, Y., Chen, G., Wan, Q., Wang, K., Zhang, J., et al. (2017). Activation of E-prostanoid 3 receptor in macrophages facilitates cardiac healing after myocardial infarction. *Nat. Commun.* 8, 14656. doi:10.1038/ncomms14656

Tunctan, B., Kucukkavruk, S. P., Temiz-Resitoglu, M., Guden, D. S., Sari, A. N., and Sahan-Firat, S. (2018). Bexarotene, a selective RXRα agonist, reverses hypotension associated with inflammation and tissue injury in a rat model of septic shock. *Inflammation* 41, 337–355. doi:10.1007/s10753-017-0691-5

Van Itallie, C. M., Mitic, L. L., and Anderson, J. M. (2012). SUMOylation of claudin-2. *Ann. N. Y. Acad. Sci.* 1258, 60–64. doi:10.1111/j.1749-6632.2012.06541.x

Wang, T., Fu, X., Chen, Q., Patra, J. K., Wang, D., Wang, Z., et al. (2019). Arachidonic acid metabolism and kidney inflammation. *Int. J. Mol. Sci.* 20, 3683. doi:10.3390/ijms20153683

Wang, L. N., Hu, P., and Yang, G. Y. (2017). Simultaneous quantitation of six podophyllum lignans using UPLC-MS/MS: Application to a pharmacokinetic study in rats. *J. HBUM.* 36 (05), 411–417. doi:10.13819/j.issn.1006-9674.2017.05.006

Wang, W. (2021). *Research on the mechanism of liver toxicity of podophyllotoxin based on metabolomics and proteomics technology.* doi:10.26973/d.cnki.gbjzu.2021.001088

Weaver, J. R., Holman, T. R., Imai, Y., Jadhav, A., Kenyon, V., Maloney, D. J., et al. (2012). Integration of pro-inflammatory cytokines, 12-lipoxygenase and NOX-1 in pancreatic islet beta cell dysfunction. *Mol. Cell. Endocrinol.* 358, 88–95. doi:10.1016/j.mce.2012.03.004

Xu, S., Bian, R., and Chen, X. (2002). *Experimental methodology of pharmacology.* Beijing, China: People's Medical Publishing House.

Xu, W., Wu, G., Wang, Z., and Du, X. (2007). Experience in the diagnosis and treatment ofacuteDysosmaVersipellis poisoning. *Zhejiang J. Traditional Chin. Med.* 99.

Xu, X., and Li, X. (2011). Current status of toxicological research on DysosmaVersipellis. *Asia-Pacific Tradit. Med.* 7, 158–160.

Xu, X., Xu, S., Zhu, J., and Huang, G. (2013). Pathological changes in rats with acute DysosmaVersipellis poisoning. *ournal Forensic Med.* 29, 333–336.

Xu, X., Zhang, X. A., and Wang, D. W. (2011). The roles of CYP450 epoxygenases and metabolites, epoxyeicosatrienoic acids, in cardiovascular and malignant diseases. *Adv. Drug Deliv. Rev.* 63, 597–609. doi:10.1016/j.addr.2011.03.006

Xuan, F., and Jian, J. (2016). Epigallocatechin gallate exerts protective effects against myocardial ischemia/reperfusion injury through the PI3K/Akt pathway-mediated inhibition of apoptosis and the restoration of the autophagic flux. *Int. J. Mol. Med.* 38, 328–336. doi:10.3892/ijmm.2016.2615

Yu, P., Chen, J., Chen, S., An, Z., Yang, G., and Ye, F. (2010). Analysis of 46 cases of oral poisoning of podophyllotoxin-containing traditional Chinese medicine. *Her. Med.* 29, 1518–1520.

Zhang, R., Zhang, Z., Wang, K., Zhao, L., Wang, Y., Wang, J., et al. (2023). Role and its mechanism of CYP2E1 in cardiac fibrosis in alcoholic cardiomyopathy. *J. Shanxi Med. Univ.* 54, 1217–1222. doi:10.13753/j.issn.1007-6611.2023.09.007

Zhang, T., Zhao, L.-L., Zhang, Z.-R., Fu, P.-D., Su, Z.-D., Qi, L.-C., et al. (2014). Interaction network analysis revealed biomarkers in myocardial infarction. *MolBiol Rep.* 41, 4997–5003. doi:10.1007/s11033-014-3366-4

Zhang, W., Lu, D., Dong, W., Zhang, L., Zhang, X., Quan, X., et al. (2011). Expression of CYP2E1 increases oxidative stress and induces apoptosis of cardiomyocytes in transgenic mice. *FEBS J.* 278, 1484–1492. doi:10.1111/j.1742-4658.2011.08063.x

Zhao, W., Cong, Y., Li, H.-M., Li, S., Shen, Y., Qi, Q., et al. (2021). Challenges and potential for improving the druggability of podophyllotoxin-derived drugs in cancer chemotherapy. *Nat. Prod. Rep.* 38, 470–488. doi:10.1039/d0np00041h

Zhao, Z. (2011). Quality control reseach of RHIZOMA DIPHYLLEIAE. Available at: https://kns.cnki.net/kcms2/article/abstract?v=vdPasdvfHvvC29-h36NP5GqAYyut44WkmQjhEcYVSMF_tixsS6nwUpqaijBN9Yn__BHrQEwK-YbITt64gionboWnPC9hB76OA2j7uvEiuDaMX2XRSF_KyI8X0RuSYCSGRcFDf6alM31V7UA8b_Z-eA==&uniplatform=NZKPT&language=CHS (Accessed January 8, 2024).

Zhou, Y., Khan, H., Xiao, J., and Cheang, W. S. (2021). Effects of arachidonic acid metabolites on cardiovascular health and disease. *Int. J. Mol. Sci.* 22, 12029. doi:10.3390/ijms222112029

Glossary

12(S)-HETE	12(S)-Hydroxy eicosatetraenoic acid
13(S)-ODE	13(S)-hydroxy octadecadienoic acid
14(15)-EpETE	14,15-Epoxyeicosatetraenoic acid
15(S)-HETE	15(S)-Hydroxy eicosatetraenoic acid
6-keto-PGF$_{1\alpha}$	6-keto-Prostaglandin F1alpha
eight-iso-PGF$_{2\alpha}$	eight-iso-Prostaglandin F2alpha
9(S)-ODE	9(S)-hydroxy octadecadienoic acid
AOE	Adverse Outcomes Evidence
ARA	Arachidonic acid
AST	Aspartate aminotransferase
BNP	Brain natriuretic peptide/brain natriuretic peptide
BP	Biological process
CC	Cellular component
CK	Creatine kinase
CK-MB	Creatine kinase-MB isoenzyme
CON	Control
cTNI	Cardiac troponin I
DEGs	Different expression genes
DHA	Docosahexaenoic acid
DV	*Dysosma versipellis*
GO	Gene Ontology
H&E	Hematoxylin–eosin
HIE	Harmful ingredients evidence
IPE	Injury phenotype evidence
IQR	Inter quartile range
KEGG	Kyoto Encyclopedia of Genes and Genomes
LDH	Lactate dehydrogenase
LTB$_4$	Leukotriene B4
LTD$_4$	Leukotriene D4
MF	Molecular functional
MYO/MB	myoglobin
NT-proBNP	N-terminal pro-brain natriuretic peptide
PGD$_2$	Prostaglandin D2
PGE$_2$	Prostaglandin E2
PGF$_{2\alpha}$	Prostaglandin F2alpha
PPT	Podophyllotoxin
TEC	Toxicological evidence chain
TEE	Toxic events evidence
TXB$_2$	Thromboxane B2
XIC	Extracting ion flow chromatography
α-HBD	Alpha-hydroxybutyrate dehydrogenase.